Ionics (2021) 27:853–865
https://doi.org/10.1007/s11581-020-03856-3

ORIGINAL PAPER

Nanocomposite polymer electrolytes comprising starch-lithium acetate and titania for all-solid-state supercapacitor

A. C. W. Ong[1] · N. A. Shamsuri[2] · S. N. A. Zaine[3,4] · Dedikarni Panuh[5] · M. F. Shukur[2,4]

Received: 12 October 2020 / Revised: 19 November 2020 / Accepted: 21 November 2020 / Published online: 26 November 2020
© Springer-Verlag GmbH Germany, part of Springer Nature 2020

Abstract

A nanocomposite solid polymer electrolyte (SPE) system has been prepared for application in a supercapacitor. Corn starch is used to host the ionic conduction with lithium acetate (LiOAc) salt as an ion provider. Different concentrations of nanosized titanium dioxide (TiO_2) filler have been added to analyse the influence of nanofiller addition on the conductivity and other properties of the electrolytes. Structural characterisation and complex formation have been examined by X-ray diffraction (XRD) and Fourier transform infrared (FTIR) spectroscopy, respectively. It is shown that the room temperature conductivity changes with the change in TiO_2 concentration. Adding 4 wt.% TiO_2 to the starch-LiOAc complex leads to an optimum conductivity of $(8.37 \pm 1.04) \times 10^{-4}$ S cm^{-1}. The variation in conductivity is accompanied by the change in surface morphology as observed from field emission scanning electron microscopy (FESEM) analysis. Linear sweep voltammetry (LSV) indicates that the electrochemical potential stability window of the electrolyte with 4 wt.% TiO_2 lies in the range between −2.0 and +1.9 V. A supercapacitor has been assembled using the electrolyte, and its performance has been characterised using impedance technique and cyclic voltammetry.

Keywords Starch · Polymer electrolyte · Lithium acetate · Titanium dioxide (TiO_2) · Supercapacitor

Introduction

The global demand for energy shows an increasing trend. Energy Information Administration's International Energy Outlook 2019 [1] predicted that total energy consumption in the world will continue to rise in the future. In order to cope with this situation, focus must be on generation of energy as well as efficient energy storage device. Rechargeable batteries and supercapacitors are well-known as promising energy storage devices. These devices are commonly used in vehicles, household electrical appliances and display devices. The key component of any energy devices is electrolyte that acts as a medium for conducting ions between electrodes [2]. A solid polymer electrolyte (SPE) is defined as an ion conductive polymer. They are also known as solid solvents that get hold of the ion transport properties similar to the conventional liquid ionic solution of electrolyte used in batteries and supercapacitors [3]. SPEs had gained attention among the researchers due to their promising properties in terms of flexibility and safety compared to conventional carbonate-based liquid electrolytes [4–9]. An SPE system is prepared by dissociating alkali metal salts into a polar polymer matrix. When the structure of polymer matrix ruptures, electron donor groups from polymer matrix form dative bonds with the cations from inorganic salts; when electric field is supplied, the ions are separated and migrated from one site of the chain to the other site [10, 11]. The main disadvantage of SPEs is their poor ionic conductivity. Incorporating a nanofiller into the polymer electrolyte is an effective technique to improve the ionic conductivity. It has been proven that nanofillers such as titanium dioxide (TiO_2) [12], copper oxide (CuO) [13],

✉ M. F. Shukur
mfadhlullah.ashukur@utp.edu.my

[1] Faculty of Engineering Science, Katholieke Universiteit Leuven, Kasteelpark Arenberg 1, 3001 Leuven, Belgium

[2] Department of Fundamental and Applied Sciences, Universiti Teknologi PETRONAS, 32610 Seri Iskandar, Perak, Malaysia

[3] Department of Chemical Engineering, Universiti Teknologi PETRONAS, 32610 Seri Iskandar, Perak, Malaysia

[4] Centre of Innovative Nanostructures and Nanodevices (COINN), Universiti Teknologi PETRONAS, 32610 Seri Iskandar, Perak, Malaysia

[5] Department of Mechanical Engineering, Universitas Islam Riau, Pekanbaru, Riau 28284, Indonesia

Content courtesy of Springer Nature, terms of use apply. Rights reserved.

aluminium oxide (Al_2O_3) [14], and zinc sulfide (ZnS) [15] have the potential not only in increasing the ionic conductivity of SPEs but also in stepping up both of their mechanical strength and thermal stability [7]. Among the nanofillers, TiO_2 is the best nanofiller in enhancing the ionic conductivity of SPE due to its high dielectric constant, high surface area and strong Lewis acid characteristics [16–18]. A report by Khanmirzaei and Ramesh [19] shows that rice starch-lithium iodide-TiO_2 electrolyte obtained a conductivity of 2.27×10^{-4} S cm^{-1}. Chitosan-silver nitrate-TiO_2 electrolyte was reported to obtain a conductivity of 1.18×10^{-6} S cm^{-1} [20]. According to Winie et al. [21], incorporating TiO_2 into hexanoyl chitosan-lithium perchlorate complex maximised the conductivity to 3.00×10^{-4} S cm^{-1} [21].

Nanocomposite polymer electrolyte can be applied as electrode separator in an electrical double-layer capacitor (EDLC) [22]. EDLC is a type of supercapacitor that stores energy through charge separation across the electrode-electrolyte interfaces [23, 24]. It is believed that a supercapacitor acts as a bridge across the power or energy gap between the dielectric capacitors and batteries [25]. In this study, starch-based nanocomposite polymer electrolytes incorporated with lithium acetate (LiOAc) are characterised, and the most conductive electrolyte is used in an all-solid-state supercapacitor.

Experimental

Polymer electrolyte preparation

A fixed amount (4 g) of corn starch (Sigma-Aldrich) was dissolved in 20 mL dimethyl sulfoxide (DMSO) (Fisher Scientific) solvent at 80 °C for 20 min. Meanwhile, different concentrations of anatase titanium dioxide (TiO_2) (Sigma-Aldrich, 25-nm particle size, 99.7%) were ultrasonicated in 30 mL DMSO for 30 min. Both solutions were cooled down to room temperature. LiOAc (Sigma-Aldrich) salt was added into the corn starch solution and stirred until a homogenous solution was obtained. The two solutions were then mixed and stirred for 1 h. The final solutions were then casted into different glass petri dishes and dried in an oven at 70 °C for 48 h. Prior to use, the samples were placed in a vacuumed desiccator. The weight percent of starch, LiOAc, and TiO_2 added into the polymer electrolytes and the designations are shown in Table 1.

X-ray diffraction

X-ray diffractograms of the electrolytes were recorded using Panalytical X'pert3 Powder with Cu Kα radiation (λ = 1.5406 Å). The 2θ angle was varied from 5° to 80°.

Table 1 Compositions and designations of starch-LiOAc-TiO_2-based polymer electrolytes

Designation	Starch (wt.%)	LiOAc (wt.%)	TiO_2 (wt.%)
PE-0	75.0	25.0	0
PE-2	73.5	24.5	2.0
PE-4	72.0	24.0	4.0
PE-6	70.5	23.5	6.0
PE-8	69.0	23.0	8.0
PE-10	67.5	22.5	10.0

Electrical impedance spectroscopy

Impedance measurements were conducted using the Metrohm Autolab in a frequency range of 50 to 1×10^6 Hz at an applied voltage of 10 mV at room temperature. The polymer electrolyte was sandwiched between stainless-steel electrodes of a sample holder. Bulk resistance (R_b) was obtained by analysing the Nyquist plot obtained from the EIS results. Ionic conductivity (σ) was calculated using Eq. 1:

$$\sigma = \frac{D}{AR_b} \tag{1}$$

where d is the thickness of the polymer electrolytes and A is the contact area between the electrolyte and electrodes which is 3.14 cm^2.

Fourier transform infrared

The FTIR spectra of the polymer electrolytes were recorded using a Perkin Elmer FTIR spectrometer at the wavenumber range of 550–4000 cm^{-1} to observe the functional group, and interactions occurred between the polymer host and the salt/nanofiller. The FTIR technique was performed at a resolution of 4 cm^{-1}.

Field emission scanning electron microscopy

Surface morphology of the polymer electrolytes were observed using a Zeiss SUPRA 55VP scanning electron microscope. Before being characterised, the samples were coated with a thin layer of gold using sputter coater EMITECH K550X. The measurements were conducted at room temperature under vacuum condition, using beam with accelerating voltage of 5.00 kV.

Linear sweep voltammetry measurement

Electrochemical stability window of the highest conducting electrolyte, as deduced from EIS study, was measured by LSV technique using two stainless-steel foils as the working

Content courtesy of Springer Nature, terms of use apply. Rights reserved.

and counter/reference electrodes. LSV measurement was carried out using the Metrohm Autolab at room temperature. The measurement was performed between − 3.0 and 3.0 V at a scan rate of 5 mV s^{-1}.

Preparation of electrodes

For preparation of supercapacitor electrodes, 13 g of activated carbon (RP20), 1 g of carbon black (Alfa Aesar) and 2 g of polyvinylidene fluoride (PVDF) (Aldrich) were mixed in *N*-methyl pyrrolidone (NMP) (Merck) and stirred until a homogenous slurry was formed. The final solution was doctor-bladed on an aluminium foil which acts as the current collector for the electrode. It was brought to dry in an oven at 60 °C for 1 h and kept in a desiccator containing silica gel until the usage of it.

Fabrication and characterisation of EDLC

Nanocomposite polymer electrolyte with the highest conductivity was sandwiched between a pair of activated carbon electrodes. Perspex plates were used to hold the cell. Impedance measurement of EDLC was done using the Metrohm Autolab in a frequency range of 10 mHz to 100 kHz at room temperature. Cyclic voltammetry (CV) measurements were conducted using the Metrohm Autolab in a potential range of 0–1.0 V at different scan rates.

Results and discussion

XRD analysis

Amorphousness in polymer electrolyte is the key attribute of ionic conductivity enhancement. The amorphousness of SPEs can be confirmed by the XRD studies. X-ray diffractogram of pure corn starch, lithium acetate, titanium dioxide, and polymer electrolytes with different concentration of TiO_2 are shown in Fig. 1. Crystalline peaks are observed at $2\theta = 15.0°$, 17.1°, 19.9°, and 22.4° [23] in the X-ray diffractogram of pure corn starch. This result demonstrates that corn starch is a semi-crystalline material since both diffuse and sharp diffraction peaks are present in its diffractogram. The highly intense peaks at $2\theta = 7.7°$, 10.1°, 21.1°, 26.1°, and 30.9° in the X-ray diffractogram of LiOAc powder indicates the crystalline nature of the salt. The peaks corresponding to LiOAc are not observed in Fig. 1c–h, inferring that the salt does not remain as a separate phase in the SPE indicating a complete salt dissociation in the starch matrix [26]. In the X-ray diffractogram of PE-0, only one broad peak at $2\theta = 20.0°$ appears. The peak is less intense compared to the peak at $2\theta = 19.9°$ in the X-ray diffractogram of pure corn starch. The decrease in the relative intensity of the peak as well as disappearance of some of the crystalline peaks indicates that salt-polymer complexation has occurred. This investigation shows that the crystallinity of polymer significantly changed due to the disturbances in the ordered structure of polymer chains when doped with salt [27]. The characteristics peaks of the crystal phase of TiO_2 are observed at $2\theta = 25.3°$ (101), 37.8° (104), 48.1° (200), 54.5° (105), and 62.8° (211) [18, 28, 29]. As the weight percentage of TiO_2 increases in the polymer electrolyte, the crystalline peaks of TiO_2 become prominent. The nanosized ceramic filler dispersed emulsion can penetrate the space between the polymer chains thus preventing or retarding crystallisation of the polymer due to its large surface area [26]. The obtained amorphous phase due to polymer-salt complexation in the electrolyte enhances ionic conduction while the crystalline region of the nanofiller provides strong mechanical support in the SPE [26].

Conductivity and dielectric studies

Typical Nyquist plots of the starch-LiOAc-based nanocomposite electrolytes at room temperature are illustrated in Fig. 2. Each plot consists of an inclined spike. The absence of semicircles at high-frequency region indicates that ions are the majority charge carriers which shows that the total conductivity is mainly due to conduction of ion [26]. The inclined spike at the low-frequency region is attributed to double-layer capacitance in a cell with an ion-blocking electrode configuration. The inclination of the spike is ascribed to the roughness of the electrolyte-electrode interface [30]. The R_b of the electrolyte was determined by extrapolating the intercept of this plot on the horizontal axis. It can be observed that the magnitude of R_b decreases as the TiO_2 content increases to 4 wt.%. However, when more than 4 wt.% TiO_2 is added, the bulk resistance increases. Ionic conductivity of the electrolytes was calculated using Eq. (1).

As observed in Fig. 3, the ionic conductivity of nanocomposite polymer electrolyte increases from $(4.03 \pm 0.63) \times 10^{-4}$ to $(8.37 \pm 1.04) \times 10^{-4}$ S cm^{-1} on addition of 4 wt.% TiO_2. This is attributed to the disruption of crystallinity of polymer electrolyte [7]. The Lewis acid characteristic and large surface area of TiO_2 had improved the ion mobility by providing more conducting paths [16, 18]. The polar surface groups of TiO_2 act as the centres to cross-link the corn starch segments in the nanocomposite polymer electrolyte and minimise the phenomenon of ion association [19, 30]. This process promotes the localised amorphous regions of the polymer electrolyte, thereby providing more conducting paths for the ions to get transported [16]. In addition, Lewis acid of TiO_2

Content courtesy of Springer Nature, terms of use apply. Rights reserved.

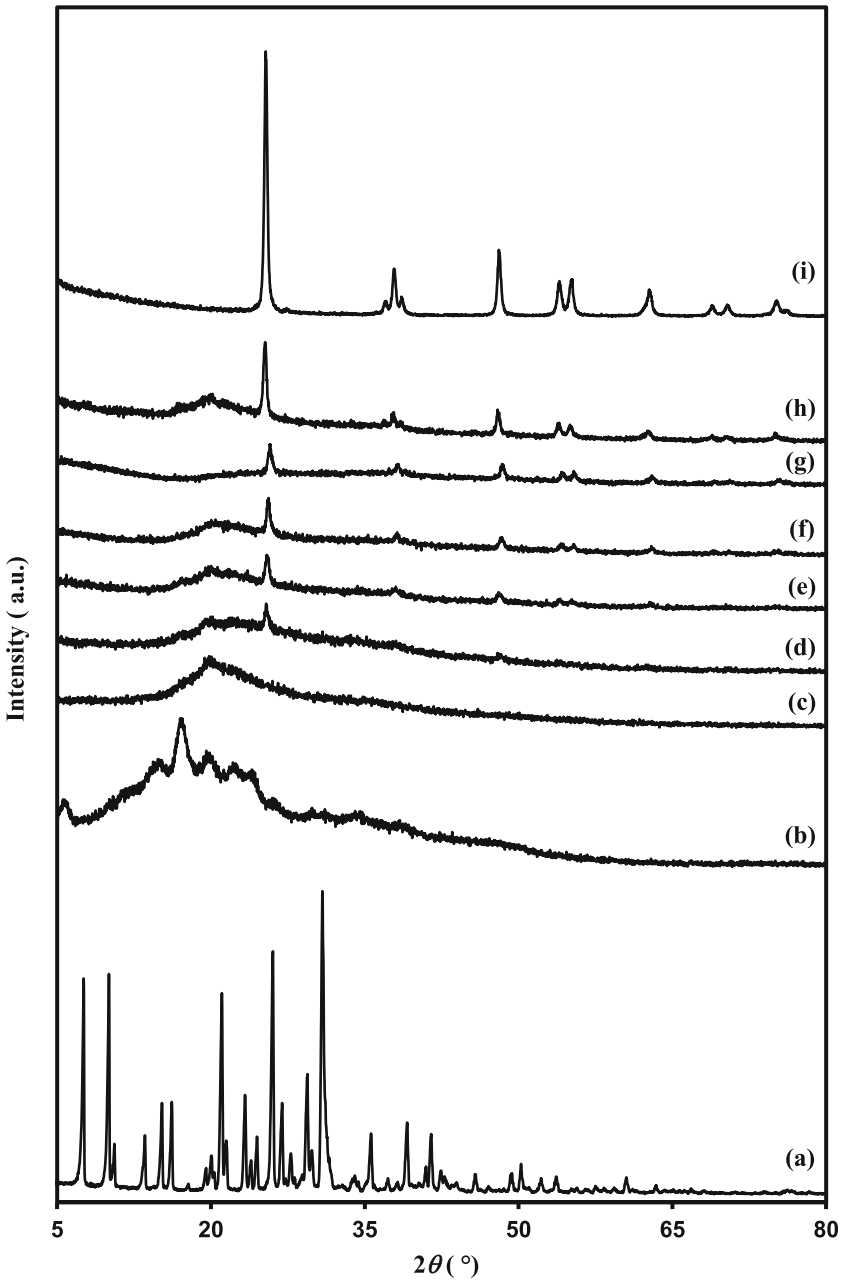

Fig. 1 X-ray diffractograms of (**a**) LiOAc salt, (**b**) corn starch, (**c**) PE-0, (**d**) PE-2, (**e**) PE-4, (**f**) PE-6, (**g**) PE-8, (**h**) PE-10, and (**i**) TiO_2

competes with Lewis acid Li^+ cation to form complexes with corn starch chain [30]. This competition enhances the mobility of ions thus giving rise to the ionic conductivity. As noticeable in Fig. 3, when the content of TiO_2 is further increased, ionic conductivity is found to be decreased. This is the result of agglomeration of TiO_2 [31]. The agglomeration of nanofillers impedes the mobile ions to migrate from one site of the chain to the other site when electric field is supplied resulting a decrease in conductivity.

Studies on alternating current conductivity or σ_{ac} spectra were done to understand the frequency-dependent conductivity behaviour of the nanocomposite polymer electrolytes. The σ_{ac} was calculated using the following equation:

$$\sigma_{ac} = \frac{d}{A}\left(\frac{Z_r}{Z_r^2 + Z_i^2}\right) \quad (2)$$

Here, Z_r is the real part of impedance and Z_i is the imaginary part of impedance. As illustrated in Fig. 4, the σ_{ac} of all the polymer electrolytes increases as frequency increases until reaching a plateau at log $f = \sim 10$ kHz. At lower-frequency region (log $f < 10$ kHz), as the frequency increases, the periodic reversal of electric field occurs at a faster rate so the ions

Content courtesy of Springer Nature, terms of use apply. Rights reserved.

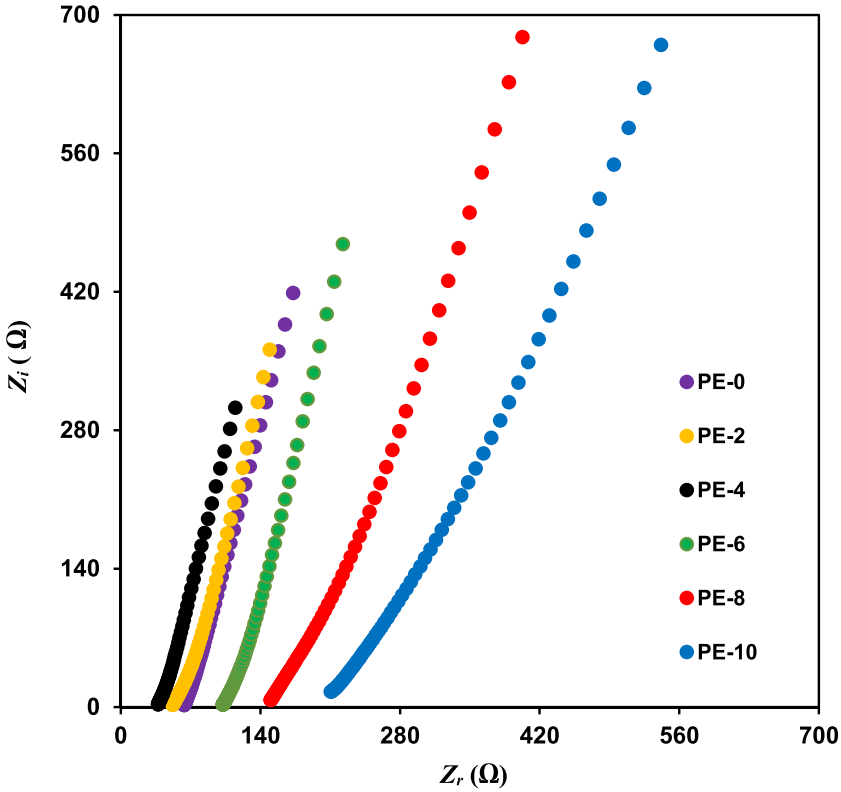

Fig. 2 Nyquist plots of starch-LiOAc nanocomposite electrolytes with different concentrations of TiO_2

move rapidly with greater mobility which result in increasing σ_{ac} [32]. The appearance of plateau at log $f = \sim 10$ kHz indicates the migration of ions from one site to the other thus contributing to the direct current conductivity (σ_{dc}). The inability of the ions to undergo consecutive hops to fit into a time scale given by roughly half a cycle also contributes to the appearance of a plateau region in the conductivity spectra of SPE [33]. The results of σ_{dc} are shown in Table 2. The results fall under the standard deviation of ionic conductivity obtained from impedance measurements and deviate less than 19% signifying that the results are in good agreement with impedance analysis.

The dependence of dielectric constant (ε_r) and dielectric loss (ε_i) on frequency for all polymer electrolytes at room

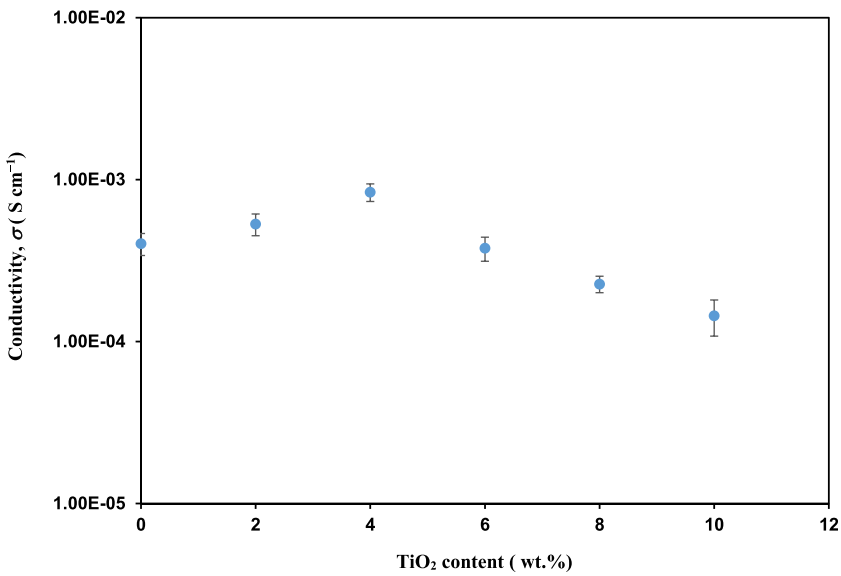

Fig. 3 The effect of TiO_2 content on the ionic conductivity

Content courtesy of Springer Nature, terms of use apply. Rights reserved.

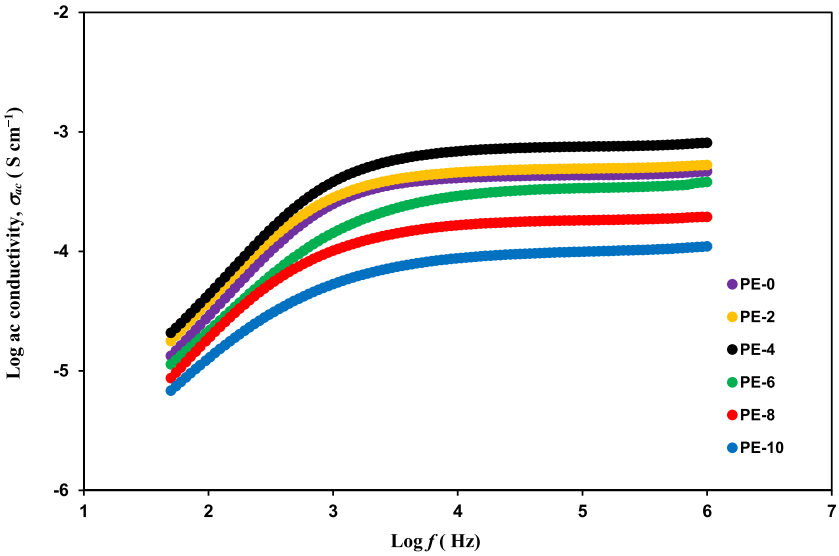

Fig. 4 The dependence of ac conductivity on frequency at room temperature

temperature are depicted in Fig. 5. The same trend is observed for all electrolytes where ε_r and ε_i decrease non-linearly with increasing frequency. At lower-frequency region, ions are accumulated at the interfaces between electrodes and electrolyte causing the existence of electrode polarisation [34]. Thus, the polymer electrolytes have higher dielectric constant. When the frequency applied is further increased, electric field reversed in a rapid rate resulting in a decrease in ion diffusion [32]. Consequently, the ions are saturated at the bulk of the sample and cause the dielectric constant to decrease. The appearance of the peak in Fig. 5b is attributed to the relaxation phenomena of the polymer due to the motion of salt-free chain segment [35].

It is obvious that PE-4 has the highest value of ε_r and ε_i, regardless of frequency. The dielectric spectra results are in good agreement with the results from ionic conductivity, confirming that ionic conductivity is mainly affected by the number density of charge carriers. When the amount of TiO_2 nanofiller is increased to 4 wt.%, the amount of charge carriers increases due to the fact that nanofiller assists the ion dissociation and eventually give rise to the dielectric constant [34]. When the concentration of TiO_2 is further increased (beyond 4 wt.%), agglomeration occurs causing ions to be impeded from being mobile leading to a decrease in dielectric constant.

Table 2 dc conductivity from ac conductivity plot

Sample	σ_{dc} (S cm^{-1})
PE-0	4.68×10^{-4}
PE-2	5.28×10^{-4}
PE-4	8.12×10^{-4}
PE-6	3.81×10^{-4}
PE-8	1.95×10^{-4}
PE-10	1.10×10^{-4}

FTIR analysis

The analysis on infrared spectra can explain the occurrence of complexation and interactions between materials which vary according to the compositions of SPEs. The FTIR spectra for pure corn starch, pure LiOAc, pure TiO_2, PE-0, and PE-4 are shown in Fig. 6. The strong and wide absorption peak centred at 3368 cm^{-1} in the spectrum of pure corn starch indicates that there are a lot of hydroxyl groups in the corn starch. The absorption peaks at 1081 cm^{-1} and 1157 cm^{-1} are attributed to C–O–H stretching vibration and C–O stretching vibration respectively [36]. The characteristic absorption of starch also appears at 930 cm^{-1} which is due to the stretching vibration of C–O in C–O–C groups [37]. It is known that adding a doping salt to the polymer host would result in the coordination of cation of the salt at the polar groups in the polymer matrix. This type of interaction influences the local structure of the polymer backbone, and certain infrared active modes of vibration will be affected [38]. In the spectrum of PE-0, the hydroxyl band peak is located at 3297 cm^{-1}, while the absorption peak due to C–O stretching vibration appears at 1150 cm^{-1}. The peak due to C–O–H stretching vibration is observed at 1080 cm^{-1}. Since the observed shift of the C–O–H stretching vibration is smaller than the resolution of the spectrophotometer, hence, the change in position of the peak is not considered a shift. The peak at 951 cm^{-1} is a result of overlapping peaks (stretching vibration of C–O in C–O–C groups and characteristic peak of LiOAc). The shifting

Content courtesy of Springer Nature, terms of use apply. Rights reserved.

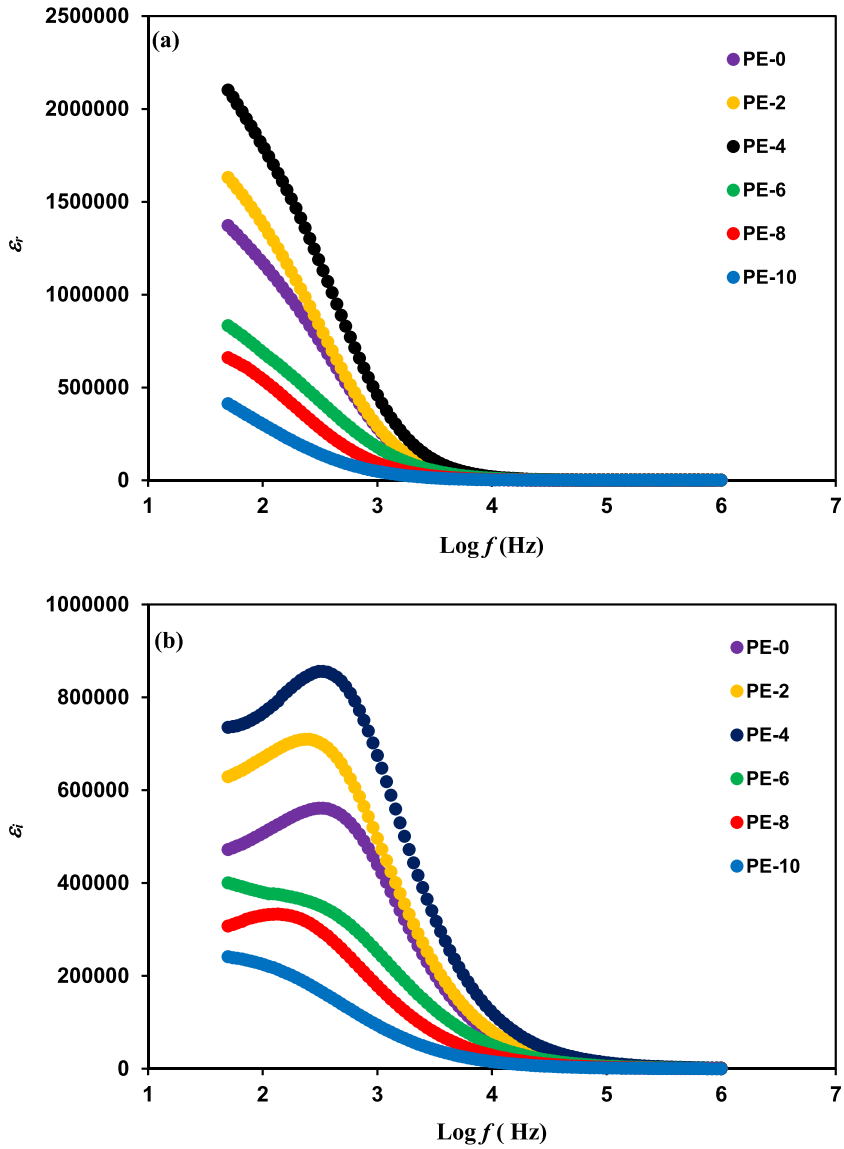

Fig. 5 Variation of (**a**) εr and (**b**) εi with frequency at room temperature

of hydroxyl band peak as well as the C–O band peak is sufficient to prove the polymer-salt complexation.

The characteristic peak of TiO_2 is observed at 1630 cm^{-1} as shown in Fig. 6e. This peak overlaps with the characteristic peak of LiOAc at 1581 cm^{-1} and H_2O bending in starch at 1647 cm^{-1} [39, 40]. The overlapping peaks result in the cage peak as can be seen in the spectrum of PE-4 in Fig. 1d. The hydroxyl band peak is observed at 3366 cm^{-1} in the spectrum of TiO_2 due to the absorbed water molecule in TiO_2 nanoparticle [41]. The presence of hydroxyl groups on the surface of nanofillers can lead to the formation of alternative conduction pathway for ions in the polymer matrix [42]. As a result, higher ionic conductivity of polymer electrolyte can be achieved. In the spectrum of PE-4, the hydroxyl band peak appears at 3293 cm^{-1}. The shifting in the position of hydroxyl band peak suggests that interaction occurs between the constituents of the electrolyte involving hydroxyl groups. This interaction can be explained using Lewis acid-base theory [16, 43]. The Lewis base in the polymer host (i.e. oxygen sites in starch) competes with Lewis base sites at the surface of TiO_2 to form complexation with the cation of salt, which is a Lewis acid. This phenomenon weakens the Coulombic force between anion and cation of LiOAc thus increasing the rate of salt dissociation [12]. Hence, more cations are available to coordinate at the oxygen atoms of hydroxyl groups. Meanwhile, hydrogen bond interaction may occur between the hydroxyl groups of TiO_2 and hydroxyl groups of starch [44]. No C–O band peak shifting is observed

Content courtesy of Springer Nature, terms of use apply. Rights reserved.

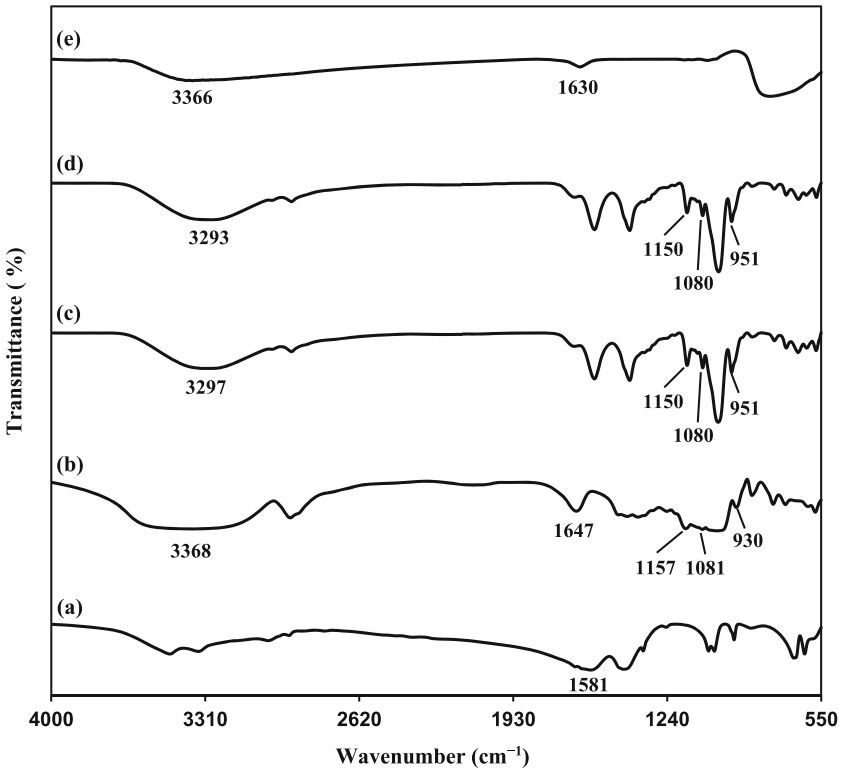

Fig. 6 FTIR spectra of (**a**) LiOAc salt, (**b**) corn starch, (**c**) PE-0, (**d**) PE-4, and (**e**) TiO_2

indicating that starch and TiO_2 have no interaction at this band.

FESEM studies

FESEM is used to analyse the change in the surface morphology when various amounts of TiO_2 is added to the starch-based polymer electrolyte. The surface of PE-0 exhibits a porous structure as shown in Fig. 7a. The porosity of the polymer electrolyte affects the ionic conductivity as it plays an essential role in charge carrier transportation [34, 45]. However, without incorporation with TiO_2, the polymer surface had very few pores of irregular shape. It is obvious that PE-4 exhibits higher porosity compared with PE-0 as depicted in Fig. 7b. This observation implies that the addition of TiO_2 has increased the porosity of the polymer electrolyte. It can be inferred that the addition of nanofiller promotes more conducting pathway for ion migration as well as enhancing the ionic mobility since the formation of pores has a potential in creating the conducting pathway [22]. The micrographs validate the result of ionic conductivity. Further incorporation of TiO_2 up to 8 wt.% has decreased the porosity of the electrolyte. From Fig. 7c, the porous structure of PE-8 was no longer significant. The ionic conductivity of polymer electrolyte decreases when the concentration TiO_2 is more than 4 wt.% as displayed in Fig. 3. This is due to the agglomeration of TiO_2 in the polymer electrolyte [30, 31]. The alteration of the surface morphology infers the occurrence of the interaction between the polymer matrix and the nanofiller via complexation as proven in the FTIR result.

LSV analysis

Prior to using the electrolyte in an energy storage device, it is essential to know the maximum voltage that can be applied on the electrolyte. LSV measurement is used to analyse the electrochemical window stability and the operational voltage of electrolytes [23, 34, 46]. In this work, stainless-steel working electrode and stainless-steel (SS) combined counter and reference electrode were used. The SS/SPE/SS cell configuration for LSV has been widely reported to determine the maximum operating voltage of SPE for the supercapacitor application [11]. The choice of stainless-steel working electrode was based on the fact that it is a ubiquitous and inexpensive material [47]. As shown in Fig. 8, the breaking voltage of PE-4 was determined by drawing a tangent to the current onset of the LSV curve and taking its intercept on the potential axis. The potential window range of PE-4 is 3.9 V, where the decomposition voltages are detected at −2.0 V (cathodic potential) and + 1.9 V (anodic potential). Shukur et al. [48] reported that starch-chitosan

Content courtesy of Springer Nature, terms of use apply. Rights reserved.

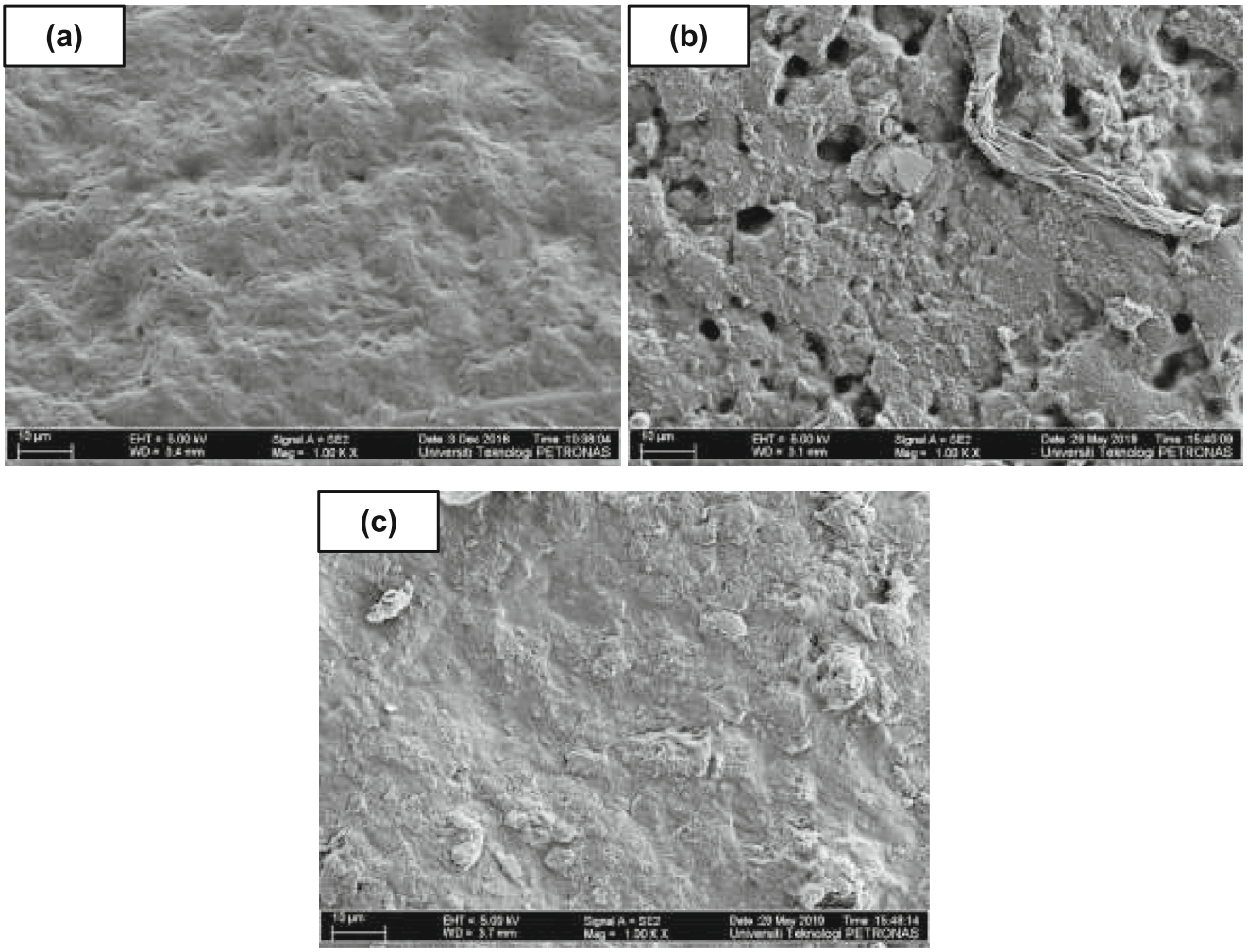

Fig. 7 FESEM micrographs of (**a**) PE-0, (**b**) PE-4, and (**c**) PE-8

blend–based electrolyte was found to decompose at 1.80 V, and the electrolyte was used in the fabrication of a supercapacitor. Decomposition voltage of 1.88 V was reported for starch-methyl cellulose blend–based electrolyte, and a supercapacitor was tested using the electrolyte [49]. The obtained result shows that the nanocomposite polymer electrolyte is safe to be used and applied in a supercapacitor.

Characterisation of the supercapacitor

EIS analysis

EIS analysis on supercapacitor was conducted to examine the bulk and interfacial resistances [22]. The Nyquist plot of the supercapacitor in Fig. 9 is displaying a semicircular arc at the high-frequency region followed by an inclined spike at the low-frequency region. The semicircular region is pictured as the construction of a parallel combination of a capacitor and a resistor [50]. The impedance measured at the highest frequency is called the equivalent series resistance (ESR). The ESR is resulted from resistances due to the polymer electrolyte, the electrodes, and the contact between the electrode and current collector [51, 52]. The diameter of the semicircle is related to the interfacial resistance that caused by the inhomogeneity interface between the electrolyte and electrodes, known as charge transfer resistance (R_{ct}). The tilted spike reveals the ion absorption at the electrolyte-electrode interfaces, thus indicating the capacitive behaviour of the supercapacitor [53]. In the present study, the recorded values for ESR and R_{ct} are 8.4 Ω and 46.1 Ω, respectively. The specific capacitance (C_s) of a single electrode is calculated using following equation [54]:

$$C_s = \frac{2}{\omega_l L m} \tag{3}$$

Content courtesy of Springer Nature, terms of use apply. Rights reserved.

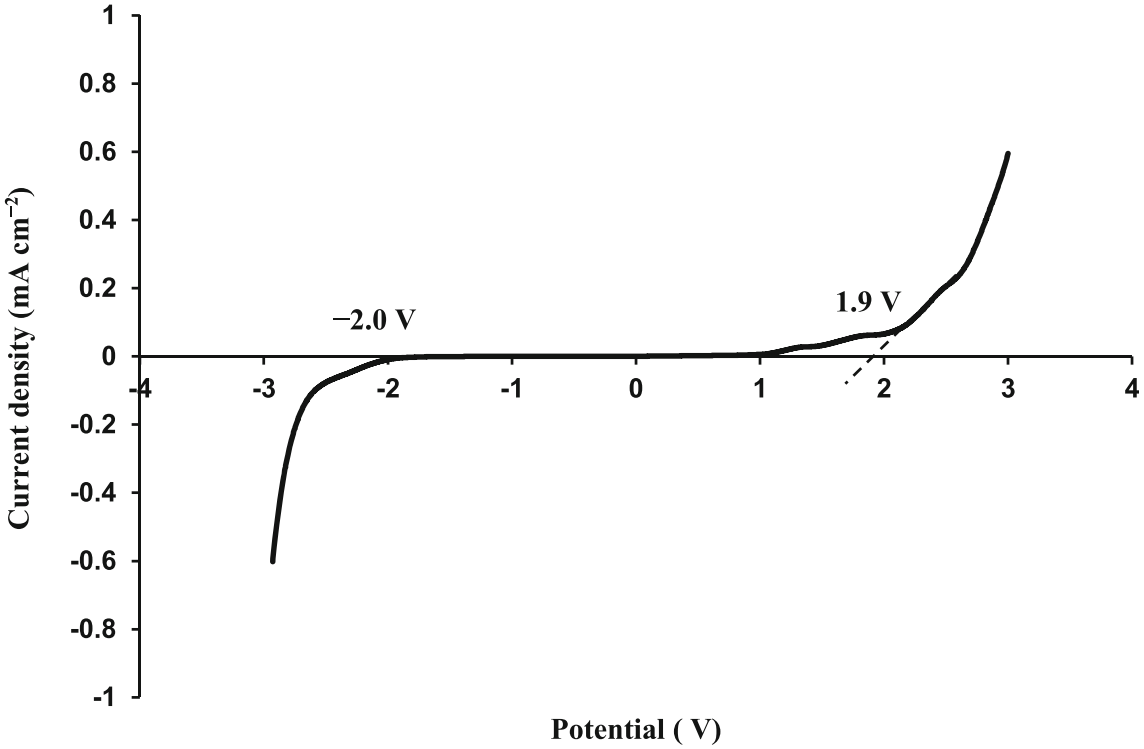

Fig. 8 LSV plot of PE-4 at 5 mV s^{-1} scan rate

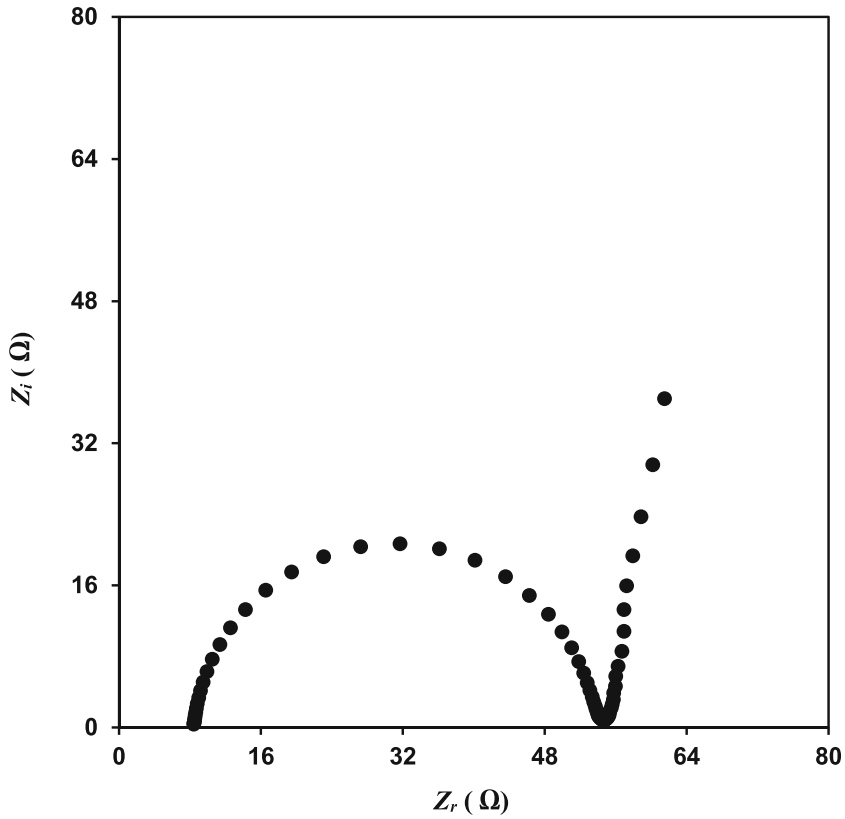

Fig. 9 Impedance plot of the supercapacitor at room temperature in the frequency range of 10 mHz to 100 kHz

Content courtesy of Springer Nature, terms of use apply. Rights reserved.

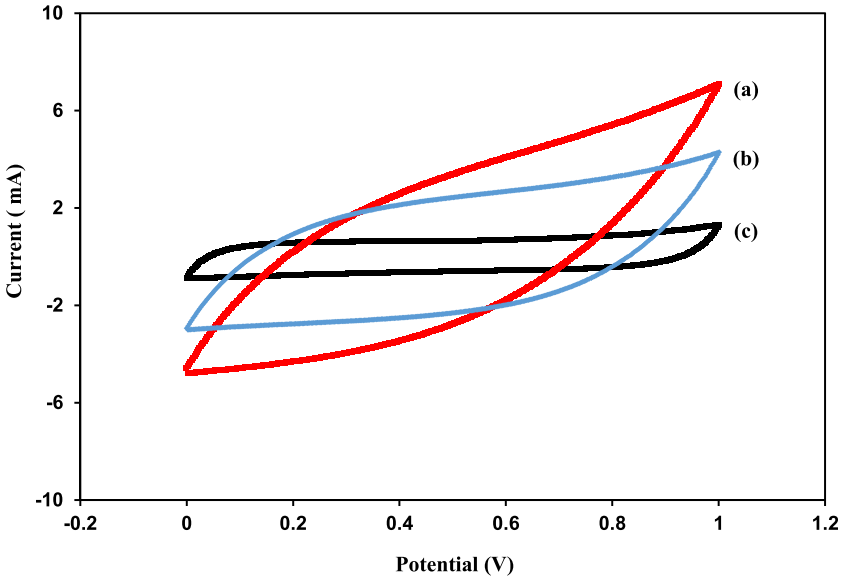

Fig. 10 CV plot at (**a**) 10, (**b**) 5, and (**c**) 1 mV s^{-1} scan rates

where ω_l is the lowest angular frequency, m is the mass of active material in an electrode, while Z_i was taken at ω_l. The C_s measured through EIS is 43.19 F g^{-1}.

CV analysis

The capacitive behaviour of a supercapacitor can also be examined using CV technique. A comprehensible comparison of cyclic voltammograms of the supercapacitor at various scan rates is shown in Fig. 10. It is observed that the shape of the cyclic voltammogram changed from leaf-shaped to a nearly rectangular shape, while the area of the plot is decreasing as the scan rate decreases from 10 to 1 mV s^{-1}. The same observation was reported in the literature [34, 48, 55]. The absence of redox peaks in the cyclic voltammograms implies that the double-layer capacitance occurs through the accumulation of ions at the interfaces between electrolyte and electrode [55]. The C_s was calculated using equation:

$$C_s = 2\int_{V_i}^{V_f} \frac{I(V)dV}{(V_f - V_i)vm} \tag{4}$$

where $I(V)$ is the current, $(V_f - V_i)$ is the range of potential, and v is the scan rate. The calculated C_s at various scan rates is tabulated in Table 3. Increasing the scan rate results in the decreasing of C_s. This is due to the presence of internal resistance. At high scan rate, the time taken by the current to reach a constant value during the reversal of the potential scan is longer. This phenomenon leads to the slow formation of electrical double-layer due to the high resistance of ionic mobility in the electrode pores [56]. At lower scan rate, ions are able to occupy the vacant sites existed at the active material on the electrode, taking into consideration that ions are provided more time to diffuse into the vacant sites which in turn leads to higher C_s [23].

Table 3 Specific capacitance of single electrode using CV measurement at different scan rates

Scan rate (mV s^{-1})	C_s (F g^{-1})
10	43.34
5	71.35
1	119.77

Conclusion

In the present work, nanocomposite polymer electrolytes were prepared using starch-based host, lithium acetate (LiOAc) salt, and TiO_2 nanofiller. From XRD studies, it was inferred that starch-LiOAc complexation enhances the amorphous phase content while the addition of the filler provides the mechanical strength. The ionic conductivity of starch-LiOAc-based electrolyte has been found to increase from $(4.03 \pm 0.63) \times 10^{-4}$ to $(8.37 \pm 1.04) \times 10^{-4}$ S cm^{-1} with the addition of 4 wt.% TiO_2. The conductivity result is validated by the ac conductivity and dielectric analysis. FTIR studies provided the evidence of Lewis acid-base interaction between the nanofiller, polymer, and salt. FESEM analysis showed that the concentration of TiO_2 affected the surface morphology of the electrolytes. Explanation based on porosity and agglomeration of TiO_2 has further strengthened the conductivity result. From LSV measurement, the nanocomposite polymer electrolyte with the highest conductivity is able to sustain the applied voltage from − 2.0 to + 1.9 V. Electrochemical performance of a supercapacitor assembled by sandwiching the electrolyte with carbon-based electrodes was analysed using EIS and CV

Content courtesy of Springer Nature, terms of use apply. Rights reserved.

techniques. Specific capacitance of a single electrode obtained from EIS is 43.19 F g^{-1}; while from CV, the highest electrode specific capacitance of 119.77 F g^{-1} is obtained at 1 mV s^{-1}. These results showed that the present nanocomposite polymer electrolyte is a good prospect for supercapacitor application.

Funding This work was supported by Universitas Islam Riau-Universiti Teknologi PETRONAS grant (015ME0-041) and YUTP grant (015LC0-048).

Compliance with ethical standards

Conflict of interest The authors declare that they have no conflict of interests.

References

1. Engineering triumph that forged a nation (2019): Panama Canal Turns 100 https://www.eia.gov/outlooks/ieo/. Accessed 12 December 2019
2. Velu SK, Raj AJ, Kalaignan PG, Thambusamy S (2018) Preparation and characterizations of PMMA-PVDF based polymer composite electrolyte materials for dye sensitized solar cell. Curr Appl Phys 18:619–625. https://doi.org/10.1016/j.cap.2018.03.014
3. Ye L, Feng Z (2010) Polymer electrolytes as solid solvents and their applications, in: C. Sequeira, D. Santos (Eds.), Polymer electrolytes: fundamentals and applications, Ch. 14, Woodhead Publishing, Cambridge, pp. 550
4. Wang Y, Fan F, Agopov AL, Yu X, Hong K, Mays J, Sokolov AP (2014) Design of superionic polymers – new insights from Walden plot analysis. Solid State Ionics 262:782–784. https://doi.org/10.1016/j.ssi.2013.09.026
5. Klongkan S, Pumchusak J (2015) Effects of nano alumina and plasticizers on morphology, ionic conductivity, thermal and mechanical properties of PEO-$LiCF_3SO_3$ solid polymer electrolyte. Electrochim Acta 161:171–176. https://doi.org/10.1016/j.electacta.2015.02.074
6. Ben HY, Garcia-Calvo O, Lago N, Devaraj S (2016) Cross-linked solid polymer electrolyte for all-solid-state rechargeable lithium batteries. Electrochim Acta 220:587–594. https://doi.org/10.1016/j.electacta.2016.10.122
7. Zhai W, Zhang Y, Wang L, Cai F, Liu X, Shi Y, Yang H (2016) Study of nano-TiO_2 composite polymer electrolyte incorporating ionic liquid PP_{1201}TFSI for lithium battery. Solid State Ionics 286:111. https://www.x-mol.com/paperRedirect/5251850
8. Lee SJ, Min HY, Gook KG, Hwan KS, Kim S, Hong K, Hyung KL (2019) Highly conductive and mechanically robust nanocomposite polymer electrolytes for solid-state electrochemical thin-film devices. Org Electron 65:426–433. https://doi.org/10.1016/j.orgel.2018.11.044
9. Aziz SB, Woo HJ, Kadir MFZ, Ahmed HM (2018) A conceptual review on polymer electrolytes and ion transport models. J Sci: Adv Mater Devices 3:1–17. https://doi.org/10.1016/j.jsamd.2018.01.002
10. Su'ait MS, Ahmad A, Hamzah H, Rahman MYA (2011) Effect of lithium salt concentrations on blended 49% poly (methyl methacrylate) grafted natural rubber and poly (methyl methacrylate) based solid polymer electrolyte. Electrochim Acta 57:123–131. https://doi.org/10.1016/j.electacta.2011.06.015
11. Aziz SB, Abdulwahid RT, Hamsan MH, Brza MA, Abdullah RM, Kadir MFZ, Muzakir SK (2019) Structural, impedance, and EDLC characteristics of proton conducting chitosan based polymer blend electrolytes with high electrochemical stability. Molecules 24:3508. https://doi.org/10.3390/molecules24193508
12. Vignarooban K, Dissanayake MAKL, Albinsson I, Mellander BE (2014) Effect of TiO_2 nano-filler and EC plasticizer on electrical and thermal properties of poly(ethylene oxide) (PEO) based solid polymer electrolytes. Solid State Ionic 266:25–28. https://doi.org/10.1016/j.ssi.2014.08.002
13. Johan MR, Fen LB (2010) Combined effect of CuO nanofillers and DBP plasticizer on ionic conductivity enhancement in the solid polymer electrolyte PEO-$LiCF_3SO_3$. Ionics 16:335–338. https://doi.org/10.1007/s11581-009-0406-5
14. Johnsi MS, Suthanthiraraj SA (2018) Effect of alumina nanofiller and diphenyl phthalate plasticizer on a silver ion conducting polyethylene oxide based nanocomposite solid polymer electrolyte. Macromol Res 26:100–106. https://doi.org/10.1007/s13233-018-6019-y
15. Dey A, Karan S, De SK (2009) Effect of nanofillers on thermal and transport properties of potassium iodide-polyethylene oxide solid polymer electrolyte. Solid State Commun 149:1282–1287. https://doi.org/10.1016/j.ssc.2009.05.021
16. Croce F, Appetecchi GB, Persi L, Scrosati B (1998) Nanocomposite polymer electrolytes for lithium batteries. Nature 394:456–458. https://doi.org/10.1038/28818
17. Rathod SG, Bhajantri RF, Ravindrachary V, Sheela T, Pujari PK, Naik J, Poojary B (2015) Pressure sensitive dielectric properties of TiO_2 doped PVA/CN-Li nanocomposite. J Polym Res 22:1–14. https://doi.org/10.1007/s10965-015-0657-y
18. Pal P, Ghosh A (2017) Influence of TiO_2 nano-particles on charge carrier transport and cell performance of PMMA-$LiClO_4$ based nano-composite electrolytes. Electrochim Acta 260:157–167. https://doi.org/10.1016/j.electacta.2017.11.070
19. Khanmirzaei MH, Ramesh S (2014) Nanocomposite polymer electrolyte based on rice starch/ ionic liquid/ TiO_2 nanoparticles for solar cell application. Measurement 58:68–72. https://doi.org/10.1016/j.measurement.2014.08.009
20. Aziz SB, Karim WO, Ghareeb HO (2020) The deficiency of chitosan: $AgNO_3$ polymer electrolyte incorporated with titanium dioxide filler for device fabrication and membrane separation technology. Journal of Materials Research and Technology 9:4692–4705. https://doi.org/10.1016/j.jmrt.2020.02.097
21. Winie T, Han CC, Subban RHY (2011) Ac conductivity and dielectric properties of hexanoyl chitosan-$LiClO_4$-TiO_2 composite polymer electrolytes. Adv Mater Res 335–336:873–880. https://doi.org/10.4028/www.scientific.net/AMR.335-336.873
22. Lim CS, Teoh KH, Liew CW, Ramesh S (2014) Capacitive behaviour studies on electrical double layer capacitor using poly (vinyl alcohol)-lithium perchlorate based polymer electrolyte incorporated with TiO_2. Mater Chem Phys 143:661–667. https://doi.org/10.1016/j.matchemphys.2013.09.051
23. Shukur MF, Ithnin R, Kadir MFZ (2014) Electrical characterizaton of corn starch – LiOAc electrolytes and application in electrochemical double layer capacitor. Electrochim Acta 136:204–216. https://doi.org/10.1016/j.electacta.2014.05.075
24. Atlas I, Ramon GZ (2018) Periodic energy conversion in an electric-double-layer capacitor. J Colloid Interface Sci 530:675–685. https://doi.org/10.1016/j.jcis.2018.06.034
25. Kim BK, Sy S, Yu A, Zhang J (2015) Electrochemical supercapacitors for energy storage and conversion. In: Yan J (ed) Handbook of clean energy systems, Vol. 5, Wiley
26. Pradeepa P, Edwinraj S, Prabhu MR (2015) Effects of ceramic filler in poly (vinyl chloride)/poly (ethyl methacrylate) based polymer blend electrolytes. Chin Chem 26:1191–1196. https://doi.org/10.1016/j.cclet.2015.05.007
27. Aziz SB, Abdullah OG, Rasheed MA, Ahmed HM (2017) Effect of high salt concentration (HSC) on structural, morphological, and

Content courtesy of Springer Nature, terms of use apply. Rights reserved.

electrical characteristics of chitosan based solid polymer electrolytes. Polymers 9:187.10.3390%2Fpolym9060187
28. El-Sherbiny S, Morsy F (2014) Synthesis, characterization and application of TiO_2 nanopowders as special paper coating pigment. Appl Nanosci 4:305–313. https://doi.org/10.1007/s13204-013-0196-y
29. Zaine SNA, Mastan AAK, Ahmedullah SS, Mohamed NM, Ahmad IA, Ramli A (2011) Synthesis and characterization of pure anatase TiO_2 aggregates. J Appl Sci 11:1326–1330 https://doi.org/10.3923/jas.2011.1326.1330
30. Ravi M, Kiran KK, Madhu VM, Narasimha VVRR (2014) Effect of nano TiO_2 filler on the structural and electrical properties of PVP based polymer electrolyte films. Polym Test 33:152–160. https://doi.org/10.1016/j.polymertesting.2013.12.002
31. Jeon J, Kim M, Kwak S (2006) Effects of addition of TiO_2 nanoparticles on mechanical properties and ionic conductivity of solvent-free polymer electrolytes based on porous P(VdF-HFP)/P(EO-EC) membranes. J Power Sources 162:1304–1311. https://doi.org/10.1016/j.jpowsour.2006.08.022
32. Teoh KH, Lim CS, Ramesh S (2014) Lithium ion conduction in corn starch based solid polymer electrolytes. Measurement 48:87–95. https://doi.org/10.1016/j.measurement.2013.10.040
33. Chatterjee B, Kulshrestha N, Gupta PN (2016) Nano composite solid polymer electrolytes based on biodegradable polymers starch and poly vinyl alcohol. Measurement 82:490–499. https://doi.org/10.1016/j.measurement.2016.01.022
34. Shukur MF, Ithnin R, Illias HA, Kadir MFZ (2013) Proton conducting polymer electrolyte based on plasticized chitosan-PEO blend and application in electrochemical devices. Opt Mater 35:1834–1841. https://doi.org/10.1016/j.optmat.2013.03.004
35. Pradhan DK, Naresh R, Choudhary P (2008) Studies of dielectric relaxation and AC conductivity behavior of plasticized polymer nanocomposite electrolytes. Int J Electrochem Sci 3:597–608
36. Teoh KH, Ramesh S, Arof AK (2012) Investigation on the effect of nanosilica towards corn starch–lithium perchlorate-based polymer electrolytes. J Solid State Electrochem 16:3165–3170. https://doi.org/10.1007/s10008-012-1741-4
37. Kibar EAA, Ferhunde U (2014) Evaluation of structural properties of cellulose ether-corn starch based biodegradable films. Int J Polym Mater 63:342–351. https://doi.org/10.1080/00914037.2013.845190
38. Sarada BA, Bhargav PB, Sharma AK, Rao VVRN (2011) Studies on (PEO+PVA+KIO_3) polymer blend electrolyte films for electrochemical cell applications. Mater Res Innov 15:394–400. https://doi.org/10.1179/143307511x13189528030753
39. Navaratnam S, Ramesh K, Ramesh S, Sanusi A, Basirun WJ, Arof AK (2015) Transport mechanism studies of chitosan electrolyte systems. Electrochim Acta 175:68–73. https://doi.org/10.1016/j.electacta.2015.01.087
40. Hassan MF, Azimi NSN, Kamarudin KH, Sheng CK (2018) Solid polymer electrolytes based on starch-magnesium sulphate: study on morphology and electrical conductivity. ASM Sci J, Spec. Issue 2018:17–28
41. Prasanna CMS, Suthanthiraraj SA (2019) Investigations of zinc ion dissociation in gel polymer electrolytes based on poly(vinyl chloride) and poly(ethyl methacrylate) blend on the addition of two different ceramic nanofillers. J Inorg Organomet Polym Mater 29:483–501. https://doi.org/10.1007/s10904-018-1021-6
42. Sun CC, You AH, Teo LL, Thong LW (2018) Effect of Al_2O_3 in poly (methyl methacrylate) composite polymer electrolytes. AIP Conference Proc 1958 020028: 1–7.doi:https://doi.org/10.1063/1.5034559
43. Wieczorek W, Florjanczykt Z, Stevens JR (1995) Composite polyether based solid electrolytes. Electrochim Acta 40:2251–2258. https://doi.org/10.1016/0013-4686(95)00172-B
44. Polu AR, Rhee HW (2016) Effect of TiO_2 nanoparticles on structural, thermal, mechanical and ionic conductivity studies of PEO_{12}–LiTDI solid polymer electrolyte. J Ind Eng Chem 37:347–353. https://doi.org/10.1016/j.jiec.2016.03.042
45. Xi J, Qiu X, Li J, Tang X, Zhu W, Chen L (2006) PVDF-PEO blends based microporous polymer electrolyte: effect of PEO on pore configurations and ionic conductivity. J Power Sources 157:501–506. https://doi.org/10.1016/j.jpowsour.2005.08.009
46. Syahidah SN, Majid SR (2013) Super-capacitive electro-chemical performance of polymer blend gel polymer electrolyte (GPE) in carbon-based electrical double-layer capacitors. Electrochim Acta 112:678–685. https://doi.org/10.1016/j.electacta.2013.09.008
47. Zhang GR, Shen LL, Schmatz P, Krois K, Etzold BJM (2020) Cathodic activated stainless steel mesh as a highly active electrocatalyst for the oxygen evolution reaction with self-healing possibility. Journal of Energy Chemistry 49:153–160. https://doi.org/10.1016/j.jechem.2020.01.025
48. Shukur MF, Ithnin R, Kadir MFZ (2014) Protonic transport analysis of starch-chitosan blend based electrolytes and application in electrochemical device. Mol Cryst Liq Cryst 603:52–65. https://doi.org/10.1080/15421406.2014.966259
49. Hamsan MH, Shukur MF, Kadir MFZ (2017) NH_4NO_3 as charge carrier contributor in glycerolized potato starch-methyl cellulose blend-based polymer electrolyte and the application in electrochemical double-layer capacitor. Ionics 23:3429–3453. https://doi.org/10.1007/s11581-017-2155-1
50. Liew CW, Ramesh S, Arof AK (2015) Characterization of ionic liquid added poly (vinyl alcohol)-based proton conducting polymer electrolytes and electrochemical studies on the supercapacitors. Int J Hydrog Energy 40:852–862. https://doi.org/10.1016/j.ijhydene.2014.09.160
51. Li Q, Zhu YQ, Eichhorn SJ (2018) Structural supercapacitors using a solid resin electrolyte with carbonized electrospun cellulose/carbon nanotube electrodes. J Mater Sci 53:14598–14607. https://doi.org/10.1007/s10853-018-2665-x
52. Barzegar F, Bello A, Momodu D, Madito MJ, Dangbegnon J, Manyala N (2016) Preparation and characterization of porous carbon from expanded graphite for high energy density supercapacitor in aqueous electrolyte. J Power Sources 309:245–253. https://doi.org/10.1016/j.jpowsour.2016.01.097
53. Liew CW, Ramesh S, Arof AK (2014) Good prospect of ionic liquid based-poly(vinyl alcohol) polymer electrolytes for supercapacitors with excellent electrical, electrochemical and thermal properties. Int J Hydrog Energy 39:2953–2963. https://doi.org/10.1016/j.ijhydene.2013.06.061
54. Farma R, Deraman M, Awitdrus TIA, Omar R, Manjunatha JG, Ishak MM, Basri NH, Dolah BNM (2013) Physical and electrochemical properties of supercapacitor electrodes derived from carbon nanotube and biomass carbon. Int J Electrochem Sci 8:257–273
55. Shukur MF, Kadir MFZ (2015) Hydrogen ion conducting starch-chitosan blend based electrolyte for application in electrochemical devices. Electrochim Acta 158:152–165. https://doi.org/10.1016/j.electacta.2015.01.167
56. Liew CW, Ramesh S, Arof AK (2016) Enhanced capacitance of EDLCs (electrical double layer capacitors) based on ionic liquid-added polymer electrolytes. Energy 109:546–556. https://doi.org/10.1016/j.energy.2016.05.019

Publisher's note Springer Nature remains neutral with regard to jurisdictional claims in published maps and institutional affiliations.

Content courtesy of Springer Nature, terms of use apply. Rights reserved.

Terms and Conditions

Springer Nature journal content, brought to you courtesy of Springer Nature Customer Service Center GmbH (“Springer Nature”).
Springer Nature supports a reasonable amount of sharing of research papers by authors, subscribers and authorised users (“Users”), for small-scale personal, non-commercial use provided that all copyright, trade and service marks and other proprietary notices are maintained. By accessing, sharing, receiving or otherwise using the Springer Nature journal content you agree to these terms of use (“Terms”). For these purposes, Springer Nature considers academic use (by researchers and students) to be non-commercial.
These Terms are supplementary and will apply in addition to any applicable website terms and conditions, a relevant site licence or a personal subscription. These Terms will prevail over any conflict or ambiguity with regards to the relevant terms, a site licence or a personal subscription (to the extent of the conflict or ambiguity only). For Creative Commons-licensed articles, the terms of the Creative Commons license used will apply.
We collect and use personal data to provide access to the Springer Nature journal content. We may also use these personal data internally within ResearchGate and Springer Nature and as agreed share it, in an anonymised way, for purposes of tracking, analysis and reporting. We will not otherwise disclose your personal data outside the ResearchGate or the Springer Nature group of companies unless we have your permission as detailed in the Privacy Policy.
While Users may use the Springer Nature journal content for small scale, personal non-commercial use, it is important to note that Users may not:

1. use such content for the purpose of providing other users with access on a regular or large scale basis or as a means to circumvent access control;
2. use such content where to do so would be considered a criminal or statutory offence in any jurisdiction, or gives rise to civil liability, or is otherwise unlawful;
3. falsely or misleadingly imply or suggest endorsement, approval , sponsorship, or association unless explicitly agreed to by Springer Nature in writing;
4. use bots or other automated methods to access the content or redirect messages
5. override any security feature or exclusionary protocol; or
6. share the content in order to create substitute for Springer Nature products or services or a systematic database of Springer Nature journal content.

In line with the restriction against commercial use, Springer Nature does not permit the creation of a product or service that creates revenue, royalties, rent or income from our content or its inclusion as part of a paid for service or for other commercial gain. Springer Nature journal content cannot be used for inter-library loans and librarians may not upload Springer Nature journal content on a large scale into their, or any other, institutional repository.
These terms of use are reviewed regularly and may be amended at any time. Springer Nature is not obligated to publish any information or content on this website and may remove it or features or functionality at our sole discretion, at any time with or without notice. Springer Nature may revoke this licence to you at any time and remove access to any copies of the Springer Nature journal content which have been saved.
To the fullest extent permitted by law, Springer Nature makes no warranties, representations or guarantees to Users, either express or implied with respect to the Springer nature journal content and all parties disclaim and waive any implied warranties or warranties imposed by law, including merchantability or fitness for any particular purpose.
Please note that these rights do not automatically extend to content, data or other material published by Springer Nature that may be licensed from third parties.
If you would like to use or distribute our Springer Nature journal content to a wider audience or on a regular basis or in any other manner not expressly permitted by these Terms, please contact Springer Nature at

onlineservice@springernature.com